J. Biomechanics Vol. 25, No. 2, pp. 129–144, 1992.
Printed in Great Britain

0021-9290/92 $5.00 + .00

GEOMETRY PARAMETERS FOR MUSCULOSKELETAL MODELLING OF THE SHOULDER SYSTEM

F. C. T. VAN DER HELM,* H. E. J. VEEGER,† G. M. PRONK,* L. H. V. VAN DER WOUDE† and R. H. ROZENDAL†

* Man–Machine Systems Group, Laboratory for Measurement and Control, Delft University of Technology, Delft, The Netherlands and † Faculty of Human Movement Sciences, Free University, Amsterdam, The Netherlands

Abstract—A dynamical finite-element model of the shoulder mechanism consisting of thorax, clavicula, scapula and humerus is outlined. The parameters needed for the model are obtained in a cadaver experiment consisting of both shoulders of seven cadavers. In this paper, in particular, the derivation of geometry parameters from the measurement data is described. The results for one cadaver are presented as a typical example.

Morphological structures are modelled as geometrical forms. Parameters describing this form are estimated from 3-D position coordinates of a large number of datapoints on the morphological structure, using a least-squares criterion. Muscle and ligament attachments are represented as a plane or as a (curved) line. Muscle paths are determined by a geometrical form of the bony contour around which the muscle is wrapped. Muscle architecture is determined by the distribution of muscle bundles over the attachment area, mapping the distribution of the origin to the insertion. Joint rotation centers are derived from articular surfaces. Hence, muscle moment arms can be calculated. The result of this study is a set of parameters for each cadaver, describing very precisely the geometry of the shoulder mechanism. This set allows positioning of muscle force vectors *a posteriori*, and recalculation of position coordinates and moment arms for any position of the shoulder.

INTRODUCTION

Dynamical finite-element model

The shoulder mechanism is a constellation of bones, i.e. thorax, clavicula, scapula and humerus, which forms the connection between the trunk and upper extremity. Since motions of these bones are closely related, the shoulder mechanism should be studied as a whole (Inman *et al.*, 1944). In the late 19th and early 20th century, Mollier (1899), Shiino (1913) and Hvorslev (1927) have built physical models of the shoulder mechanism, based on shoulder specimens. They replaced muscles on a cadaver by cords running from origin to insertion. Changes in muscle length could be established by changes in cord length and have been described extensively. Maximal muscle moments were calculated using the physiological cross-sectional area (PSCA) of muscles. Since then, biomechanical models were used to calculate the muscle forces and moments. The models derived were large simplifications of the shoulder mechanism (De Luca and Forrest, 1973; Poppen and Walker, 1978; Bassett *et al.*, 1990). The arrival of powerful computers has enabled the development of more complex musculoskeletal models, e.g. of the lower limb (Brand *et al.*, 1982; Seireg and Arvikar, 1975; Pierrynowski, 1982) or the spine (Gracovetsky and Farfan, 1986). Thus far, the shoulder mechanism has been studied less extensively, probably due to the 3-D motions, the complex motion constraints caused by the scapulothoracic gliding plane and the number of links and muscles involved. Usually, only part of the mechanism, e.g. the glenohumeral joint, has been taken into account, or the role of separate morphological structures like muscles and ligaments has been described without referring to the function of the total shoulder mechanism. However, to gain insight into the role of each morphological structure in the functioning of the total mechanism, all structures should be included in one model. Therefore, a dynamical model of the shoulder mechanism has been developed using the finite-element method (Werff, 1977; Werff and Jonker, 1983; Jonker, 1988; Van der Helm, 1988; Pronk, 1989; Van der Helm and Pronk, 1989). In this finite-element model, morphological structures are represented by elements whose dynamical behavior is well known. Then, despite its complexity, equations of motion for the whole mechanism can be derived by simply connecting the elements.

In the finite-element model of the shoulder mechanism, clavicula and humerus are modelled as single, rigid BEAM elements, and the scapula as a combination of two rigid BEAM elements. The sternoclavicular, acromioclavicular and glenohumeral joints are each represented by three orthogonal HINGE elements. Muscles are modelled as one or more active TRUSS or CURVED-TRUSS elements which deliver the force necessary for position changes and dynamic equilibrium. The costoclavicular, conoid and trapezoid ligaments are modelled as flexible, passive TRUSS elements, while the scapulothoracic gliding plane is modelled by two SURFACE elements, which constrain the motions of two points at the medial border of the scapula. Finally, mass and rotational inertia of segments are represented by lumped inertia at the

Received in final form 2 *July* 1991.

nodes, while external forces (e.g. gravity) also act at these nodes. With above assumptions, the shoulder mechanism model has seven degrees of freedom: four at the scapula and three at the humerus. For simulation, the input variables of the model will be the prescribed (measured) position, velocity and acceleration of bony landmarks. The output will be the calculated stress in muscles (active TRUSS elements) using an optimization criterion.

Determination of parameters

A cadaver study is performed in order to acquire data for inertia, geometry and muscle contraction parameters of the dynamical finite-element model of the shoulder mechanism described (Veeger *et al.*, 1991). In general, the number and nature of parameters included in a model depend on the sort of model, the characteristics of the system to be modelled and the availability of measurement techniques to derive an accurate estimation of the parameters. In the finite-element method, the most important characteristics of the shoulder mechanism can be included. To describe the geometry of the shoulder mechanism, the parameters of the following morphological structures are defined:

—The location of origin and insertion of all muscles.

—The shape and position of bony contours determining the muscle path.

—The location of the attachments of the costoclavicular, conoid and trapezoid ligaments.

—The location of the joint rotation centers of the sternoclavicular, acromioclavicular and glenohumeral joints.

—The shape and position of the scapulothoracic gliding plane.

—The position of well-defined bony landmarks.

In this study, a large number of datapoints located on morphological structures are measured using a new instrument: the palpator (Pronk and Van der Helm, 1991; Veeger *et al.*, 1991). The palpator is a spatial digitizer which consists of four links connected by four hinge joints. Rotations of these joints are recorded using high-precision potentiometers and, hence, the position of the endpoint of the final link can be calculated. Spatial coordinates are measured by simply touching the palpator's endpoint to a point and pressing a trigger. Morphological structures can subsequently be described mathematically by geometrical forms, which are fitted to the datapoints using a least-squares criterion.

In our dynamical finite-element model, the muscles are represented by active TRUSS elements, ligaments by passive TRUSS elements, while the joints are represented by HINGE elements and the scapulothoracic gliding plane by SURFACE elements. Parameters describing the positions and orientations as well the dynamic properties of elements are required. These parameters are derived from the recorded datapoints. For each morphological structure, it will be discussed which characteristics have been implemented in the model.

Muscles. In the finite-element model, a muscle is represented by one or more active TRUSS elements. For an adequate representation of muscle action, the following items must be considered:

(1) The number of force vectors (elements) as well as their positions and directions.

(2) Whether or not a muscle should be represented by curved muscle lines of action.

(3) The contraction characteristics, i.e. characteristics affecting the magnitude of each force vector.

Number, position and direction of force vectors. Most authors (e.g. Mollier, 1899; Shiino, 1913; Hvorslev, 1927; Gracovetsky *et al.*, 1981; De Luca and Forrest, 1973; Pierrynowski, 1982; Hogfors *et al.*, 1987; Wood *et al.*, 1989a, b) divide large muscles into convenient portions, which represent more or less functionally distinguishable parts. Each part is modelled with one muscle line of action. Large attachment sites are sometimes represented by optically estimated centroids (Hogfors *et al.*, 1987). Only Scholten *et al.* (1982) defined an arbitrary, large number of elements (18) to represent the function of the m. deltoideus. Both procedures have several disadvantages: (i) the correctness of the chosen points can never be ascertained afterwards; (ii) there is no theory which defines a minimum or maximum number of force vectors representing the muscle action; and (iii) the effect of the chosen location and direction of the force vector on the calculated muscle force is unknown.

When a muscle has a clearly distinguishable tendon, it can be assumed that the muscle force vector is positioned at one point representing the attachment of the tendon. However, when the muscle has a large attachment site, the position and direction of the muscle force vector is not clear. Obviously, in musculoskeletal modelling, the number and position of muscle lines of action affect the force attributed to the muscle. Each muscle exerts a moment around a joint. The muscle force at the attachment site is one force component of the torque couple, normally; the joint reaction force being the other. However, if the attachment area of a muscle is sufficiently large and parts of the muscle with different bundle orientations contract with different directions of force, then one muscle by itself can provide the two force components of a torque couple and exert a rotating moment on a bony segment. Clearly, such a muscle should not be represented by just one force vector but must be represented by two or more force vectors.

An example in the shoulder region is the m. trapezius, of which the laterally rotating moment cannot be ignored (Fig. 1). In order to represent such large muscles adequately, the total attachment area has to be mathematically described. One cannot settle just for the center of the area. Then the muscle force vectors (i.e. active TRUSS elements) can be positioned afterwards.

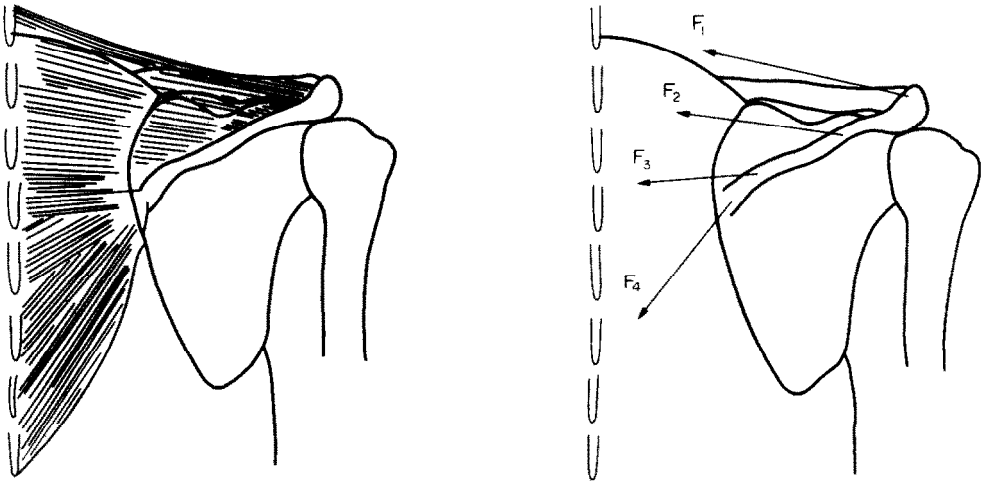

Fig. 1. The laterally rotating torque of the m. trapezius. When the m. trapezius is represented with one force vector, the torque can never be modelled; with two or more force vectors, the distribution over the attachment site and direction of the force vectors is critical for muscle force calculations.

Table 1. The muscle line of action of the following muscles is determined by a bony contour. In the last column the geometrical form used to model the bony contour is presented

Muscle	Bony contour	Geometrical form
M. serratus anterior	Thorax	Ellipsoid
M. deltoideus	Tuberculum majus & minus	Sphere
M. pectoralis major	Humeral shaft	Cylinder
M. latissimus dorsi	Humeral shaft	Cylinder
M. teres major	Humeral shaft	Cylinder
M. infraspinatus	Caput humeri	Sphere
M. supraspinatus	Caput humeri	Sphere
M. subscapularis	Caput humeri	Sphere
M. biceps, long head	Sulcus intertubercularis	Line

In the current study, the attachment area of a muscle has been recorded by a large number of datapoints. This area is described mathematically by a geometrical form (e.g. a curved line or a plane), which was fitted to datapoints using a least-squares criterion.

The force vectors (active TRUSS elements) can then be positioned afterwards to represent muscle action. The direction of force vectors depends on the orientation of muscle bundles. Thus, if a bundle orientation, i.e. the position of the origin and insertion of the bundle, is known, the direction of the force vector is clear. For this reason, during dissection, a number of muscle bundles has been marked at origin and insertion with colored beads (Veeger *et al.*, 1991). The distribution of these beads over both attachment sites enabled the mapping of bundles from origin to insertion. By means of this distribution, the direction of force vectors in our model can be calculated (Van der Helm and Veenbaas, 1991).

Curved muscle lines of action. For some muscles, the muscle line of action cannot be described by a straight line between origin and insertion, but should be defined around a bony contour. If the shape and the position of this bony contour are known, i.e. are measured and modelled, the curved line representing the muscle line of action can be calculated, assuming that the muscle is free to shift over this surface. For instance, the m. serratus anterior wraps around the thorax, which is modelled as an ellipsoid. In this approach, the thickness of the muscle belly is neglected. A complete list of muscles with curved muscle lines of action and adjoining bony contours is presented in Table 1. Also presented are the geometrical forms fitted to the bony contours.

Contraction characteristics. The magnitude of muscle force depends on a number of characteristics, e.g. the force–length and force–velocity relations, architecture, and physiological cross-sectional area (PCSA). However, those characteristics describe mainly the maximal muscle force; the factors affecting the submaximal muscle force are not precisely known as yet, but are implicitly assumed in optimization criteria as minimal use of energy, minimal joint reaction force or minimal muscle stress. Only a few of the above-

mentioned characteristics can be measured easily on cadavers, i.e. PCSA and muscle weight. The PCSA is used as an estimation of the maximal muscle force, or for calculation of muscle stress (=actual muscle force divided by PCSA). It is assumed that all muscles have been measured at the same percentage of muscle optimum length (Woittiez, 1984). The effects of change of muscle length can eventually be included, assuming that the total muscle volume does not change due to muscle contraction.

Another way to describe the same characteristics is to use muscle weight for the calculation of muscle volume. When the muscle length is measured, an approximation of the PCSA can subsequently be calculated (Fick, 1911). Data of PCSA in this cadaver study have been presented in Veeger *et al.* (1991).

Ligaments. Modelling of attachments of ligaments of the shoulder mechanism, i.e. the costoclavicular, conoid and trapezoid ligaments, is basically the same as for muscles. In consequence of the small attachment area, one (passive) TRUSS element is assumed to represent the force vector of each ligament. All ligament attachments are represented by the centroid of the attachment, and the ligament line of action by a line connecting the centroids of origin and insertion.

Joints. In the finite-element model, each joint is represented as three orthogonal HINGE joints with zero length, thus behaving as a ball-and-socket joint with three degrees of freedom and no translations.

The joint surfaces of sternoclavicular, acromioclavicular and glenohumeral joint have been measured in order to estimate the rotation center. The glenohumeral joint can be represented as a perfect ball-and-socket joint with no translation of the rotation center of the humerus with respect to the scapula (Van der Helm *et al.*, 1989). Its rotation center is located at the center of a sphere fitted to the glenoid, using a radius equal to the radius of the humeral head.

Both the sternoclavicular and acromioclavicular joint do not resemble ball-and-socket joints. However, considering the capsule of both joints, translation of the articular surfaces with respect to each other will most likely be restricted to a few millimeters. Hence, rotation will be the main degree of freedom of the joints. If translation is neglected, the rotation center can maximally shift from one edge of the articular surface to the other. Consequently, half the size of the intersection of the articular surface will be the maximum error in the estimation of the rotation center. Considering the small rotations of the joints (Pronk, 1987), the effect of these assumptions for the model will be small.

It is assumed that the medial border of the scapula is always connected to the thorax during elevation of the humerus, due to the action of the m. serratus anterior and the m. rhomboideus (Mollier, 1899). The so-called scapulothoracic gliding plane has been modelled as an ellipsoid (Pronk and Padt, 1986). This 'joint' is represented by two SURFACE elements, each constraining a point of the medial border of the scapula to an ellipsoid.

Input and output of the model. The input for a simulation of the model consists of the positions, velocities and accelerations of bony landmarks (Pronk, 1987). Hence, in the model, the positions of these landmarks are included in order to relate the observed motions to the geometry of the shoulder mechanism. The output of the model consists of the magnitude of muscle forces. Unfortunately, this output cannot be compared with direct measurements of muscle forces. Hence, the model can be validated only in a qualitative sense by comparison with the EMG of shoulder muscles for several positions and loads of the shoulder mechanism.

DATA PROCESSING

The methodology of the data collection is described in Veeger *et al.* (1991). Seven cadavers, selected on availability, are measured, totalling 14 shoulders. Three-dimensional coordinates of datapoints are defined with respect to a global coordinate system, with its origin at the incisura jugularis and the orientation of coordinate axes parallel to the main anatomical axes (x-axis: left to right; y-axis: caudal to cranial; z-axis: ventral to dorsal).

The position of an anatomical structure has been described by a geometrical form, e.g. a line or a surface, fitted to the recorded datapoints. In this study, the following geometrical forms have been used: a plane, a sphere, an ellipsoid, a (curved) line and a cylinder. The approach is the same for each form: parameters are estimated by minimizing the distance between datapoints and the geometrical form using a least-squares criterion.

In Tables 2–5, the morphological structures that have been measured are listed. These consist of 16 muscles, 3 ligaments, 6 joint surfaces, 4 bony structures which define muscle paths, and bony landmarks for comparison with *in vivo* movement registration. Also, for each structure the descriptive geometrical form is shown. Each form is chosen with three contradictory objectives: (i) to minimize the number of parameters (i.e. a low-order approximation); (ii) to adequately describe the structure by selecting a similar form; and (iii) to minimize the residual error.

For the parameter estimation of a plane, the total linear least-squares (TLLS) technique has been used (Van Huffel and Vandewalle, 1985). This technique fits a lower-dimensional subspace, in this case a plane, to the datapoints with a noise distribution over each coordinate, as distinct from an ordinary least-squares technique, which will attribute all the noise to one coordinate. The TLLS technique is suitable only if the mathematical description is linear (Appendix A). For each plane-shaped attachment, the centroid $\mathbf{C}(c_x, c_y, c_z)$ is calculated and the distributions d_x, d_y, and d_z in x-, y- and z-directions, respectively. The

Table 2. Description of the morphological structures of the thorax by geometrical forms, i.e. a point, (curved) line, plane sphere, cylinder or an ellipsoid (in mm)

Plane

	e	n_x	n_y	n_z	c_x	c_y	c_z	d_x	d_y	d_z
art_sc_th	0.87	−0.90	−0.33	−0.27	20.7	9.1	23.3	1.7	0.4	4.5
lig_cost_th	1.10	−0.08	−0.91	−0.41	57.6	7.6	23.2	2.1	0.7	1.9

Line

	e		Order 0	1	2	3	4	5	6
m_lat_dor_o	3.37	t_x	126.9	−183.1	88.7				
		t_y	−392.4	203.1	745				
		t_z	62.9	217.1	−125.4				
m_trap_o	2.60	t_x	24.9	−48.0	137.8	−177.7	66.1		
		t_y	−242.2	336.0	193.3	−287.3	118.8		
		t_z	161.1	−138.4	964.8	−1769.0	891.5		
m_rhom_o	1.61	t_x	17.5	−6.0					
		t_y	−49.6	144.0					
		t_z	177.3	−63.1					
m_lev_sca_o	0.86	t_x	29.5	−7.7					
		t_y	77.7	70.0					
		t_z	64.2	−7.5					
m_pec_maj_o	2.94	t_x	82.8	384.8	−3910.4	9460.0	−9388.8	3420.6	
		t_y	−151.4	236.8	−1898.6	5607.6	−5781.9	1994.1	
		t_z	13.4	−620.3	2432.1	−4675.7	4572.9	−1772.0	
m_pec_min_o	2.26	t_x	127.4	−124.9	48.9				
		t_y	−106.6	38.4	54.6				
		t_z	23.9	−113.3	94.1				
m_ser_ant_o	3.88	t_x	144.5	240.7	−1591.0	2512.2	−1207.4		
		t_y	−245.0	75.4	261.8	−37.5	−59.8		
		t_z	95.1	−267.4	−438.7	1511.1	−841.4		

Ellipsoid

	e	m_x	m_y	m_z	a_x	a_y	a_z
thorax	3.51	0.0	−296.2	77.8	153.0	404.2	130.0

Point

	e	x	y	z
incis_jug	—	0.0	0.0	0.0

$\bar{e}$ mean residual error.
t_x, t_y, t_z parameters of the t-polynome of x-, y- and z-coordinates, the order of the line being equal to the number of parameters minus one.
n_x, n_y, n_z normalized normal vector to the plane.
c_x, c_y, c_z coordinates of the centroid.
d_x, d_y, d_z distribution (first-order moment) of the attachment over the plane.
m_x, m_y, m_z coordinates of the center of the sphere.
r radius.
x_0, y_0 position vector of the central axis of the cylinder ($z_0=0$).
d_x, d_y, d_z normalized direction vector of the central axis.
m_x, m_y, m_z coordinates of the center of the ellipsoid ($m_x=0$).
a_x, a_y, a_z length of the x-, y- and z-axis of the cylinder.

distribution is calculated as a first-order moment around the centroid, e.g.

$$d_x=\frac{1}{A_{xy}}\int_{x_{min}}^{x_{max}}(y_{max}(x)-y_{min}(x))|x-c_x|dx$$
$$=\frac{1}{A_{xz}}\int_{x_{min}}^{x_{max}}(z_{max}(x)-z_{min}(x))|x-c_x|dx,$$

where A_{xy} is the surface area of the attachment projected onto the xy-plane, x_{min} and x_{max} are the minimum and maximum values of the contour and $y_{min}(x)$ and $y_{max}(x)$ are the minimum and maximum y-values for a certain x. Similar notations are used for z. Distributions d_y and d_z are calculated analogously.

For the nonlinear descriptions, e.g. in the case of a sphere, cylinder or ellipsoid, a somewhat different approach is used. This approach consisted of a first approximation of parameters using a linear approach,

Table 3. Description of the morphological structures of the clavicula by geometrical forms (see Table 2 for explanation)

Plane

	e	n_x	n_y	n_z	c_x	c_y	c_z	d_x	d_y	d_z
lig_con_cl	0.47	0.17	−0.99	0.01	126.7	52.3	79.0	2.8	0.5	1.9
lig_trap_cl	0.49	−0.04	−1.00	0.01	142.0	53.7	76.2	2.7	0.1	3.4
lig_costo_cl	0.28	−0.37	0.54	−0.76	49.7	23.9	26.7	6.7	2.1	1.8
art_sc_cl	1.61	−0.81	−0.46	−0.38	27.5	19.4	19.0	3.1	0.5	6.8
art_ac_cl	2.21	−0.88	0.22	0.43	155.8	57.1	83.3	2.8	5.9	2.2

Line

	e		Order 0	1	2
m_delt_o	2.40	t_x	109.6	48.9	
		t_y	53.7	5.4	
		t_z	56.6	10.6	
m_trap_i	2.15	t_x	90.6	110.0	−62.8
		t_y	58.6	13.0	−7.9
		t_z	71.2	−7.8	32.9
m_pect_maj_o	2.61	t_x	33.2	69.8	
		t_y	20.0	28.7	
		t_z	0.3	41.3	

followed by an iterative Gauss–Newton method to update the parameters until the residual error was minimal. Appendix B describes the fitting of a sphere, Appendix C, that of a cylinder, and Appendix D, that of an ellipsoid.

Appendix E describes the modelling of muscle attachments by a curved line. The x-, y- and z-coordinates are expressed as functions of the variable t ($t \in [0, 1]$). The parameters of these functions are estimated for each coordinate separately, using a least-squares criterion. Muscle architecture, i.e. bundle direction, is described by mapping the origin of muscle bundles to their insertion. Before exarticulation and the coupled cutting of muscle bellies, the origin and insertion of a number of muscle fibers have been marked with beads of the same color. In this way, the distribution of muscle bundles over attachment areas was known, so that the bundle orientation could be calculated. For each marked bundle i, the value of variable t of origin, $t_o(i)$, and insertion, $t_i(i)$, is calculated. Next, $t_o(i)$ has been fitted to $t_i(i)$ with a polynomial function, thus allowing, for each attachment point at the origin, the connected point at the insertion to be interpolated. So, for each bundle the orientation could be calculated.

RESULTS

In the cadaver study, both shoulders of the seven cadavers have been subjected to measurements, totalling 14 shoulders. It is hard to tell beforehand whether it will be possible to develop one general model with averaged model parameters, or whether the parameters have to be set for every individual shoulder. In contrast to Hogfors *et al.* (1987), scaling of geometry parameters with respect to bony dimensions did not result in a sufficient similarity of attachment shape. For a number of cadavers, intraindividual (left–right) differences were even as large as interindividual differences. In our opinion, a comparison of geometry parameters without considering the functional morphology is useless, which implies that in the scope of this article no further comparisons are discussed. Hence, it was difficult to present all results of this cadaver experiment in an interpretable fashion and we have chosen to present in Tables 2–5 the parameters describing the geometry of one cadaver (i.e. cadaver K2) with respect to its global coordinate system. Considering the inertia, geometry and muscle contraction parameters, this cadaver seemed to be a more or less median cadaver (Veeger *et al.*, 1991). (More data for other cadavers are available on request.) It should be kept in mind that the parameters presented are those corresponding to the position in which the cadaver was measured, and not to the anatomical or any other well-defined position. However, since the position of the bones can be used as an input for the model, this undefined position is not important. For each subsequent position, the coordinates can be calculated again. In Tables 2–5, the geometry parameters of the right shoulder of cadaver K2 are shown for the thorax, clavicula, scapula and humerus, respectively. The morphological structures are clustered, with respect to their geometrical forms, in a sequence: a plane, line, point, sphere, ellipsoid and cylinder.

The articular surfaces of the glenohumeral joint are modelled as a sphere. Parameters of the sphere are the coordinates of its center and its radius. As shown, the center and radius are different for the humeral head and the glenoid, due to method artifacts (estimated

Table 4. Description of the morphological structures of the scapula by geometrical forms (see Table 2 for explanation)

Plane

	e	n_x	n_y	n_z	c_x	c_z	c_y	d_x	d_y	d_z
m_infr_o	6.25	−0.71	−0.06	−0.70	120.9	−25.8	145.4	11.1	24.0	13.4
m_subsc_o	4.14	−0.70	−0.28	−0.66	114.6	−47.6	144.8	13.9	16.4	21.7
m_supr_o	3.48	−0.19	−0.91	−0.37	104.4	30.9	131.2	10.1	1.3	8.3
m_ter_min_o	0.29	−0.70	−0.16	−0.69	149.4	−42.6	118.0	2.3	9.5	4.5
m_ter_maj_o	1.75	−0.85	−0.16	−0.51	128.8	−89.0	145.0	4.9	8.5	5.4
lig_con_sc	0.02	0.03	−1.00	−0.03	126.7	34.3	81.3	4.3	0.4	−10.4
lig_trap_sc	0.23	0.23	−0.97	−0.12	133.4	37.3	74.6	2.6	1.0	2.9
art_ac_sc	0.18	−0.97	0.21	0.10	168.6	55.6	78.7	0.6	0.6	4.5

Line

			Order 0	1	2	3	4	5	6
m_delt_o	3.44	t_x	120.1	39.9	275.2	−262.1			
		t_y	7.9	88.2	−60.7	22.5			
		t_z	152.2	−71.3	−21.8	−1.4			
m_coracob_o	1.11	t_x	134.6	20.9					
		t_y	18.2	9.1					
		t_z	50.1	−5.0					
m_tric_o	3.25	t_x	152.4	21.0					
		t_y	−27.4	23.7					
		t_z	106.8	−26.4					
m_trap_i	4.43	t_x	104.1	58.3					
		t_y	13.2	46.1					
		t_z	162.5	−67.4					
m_rhom_i	2.42	t_x	108.2	−25.3					
		t_y	−116.6	133.1					
		t_z	178.0	−19.0					
m_lev_sca_i	3.00	t_x	82.7	−3.4					
		t_y	0.6	52.1					
		t_z	169.5	−57.1					
m_pec_min_i	0.95	t_x	144.7	−11.4					
		t_y	21.1	13.3					
		t_z	37.5	18.5					
m_ser_ant_i	3.73	t_x	117.1	−66.9	18.6	12.5			
		t_y	−114.5	7.9	440.2	−288.5			
		t_z	160.0	43.8	−35.6	−59.0			

Sphere

	e	m_x	m_y	m_z	r
art_gh_sc	0.44	187.3	14.9	57.6	32.0
art_gh_mgl	0.53	183.2	13.8	61.6	26.6

Point

	e	x	y	z
m_bic_cb_o	0.58	152.8	26.5	44.6
m_bic_cl_o	1.26	163.3	33.2	71.6
ts	—	86.8	0.1	163.3
ai	—	119.0	−108.5	159.9
aa	—	192.3	50.9	86.6
ac	—	165.3	58.2	95.5

transformation functions!) and restrictions on the set of datapoints (small area of the glenoid). Therefore, another fitting procedure has been performed for the center of the glenoid, using the radius of the humeral head as radius. It can be argued that the center of this sphere is the rotation center of the humerus with respect to the scapula (Van der Helm *et al.*, 1989); see Fig. 2.

The articular surfaces of the sternoclavicular and acromioclavicular joints have been modelled as a plane. Neglecting (small) translations in the joint, the shift of the rotation center from one edge of the

Table 5. Description of the morphological structures of the humerus by geometrical forms (see Table 2 for explanation)

Plane

	e	n_x	n_y	n_z	c_x	c_y	c_z	d_x	d_y	d_z
m_delt_i	3.02	−0.43	0.04	0.90	187.8	−88.8	55.6	5.4	12.1	3.1
m_coracob_i	0.39	−0.96	0.06	0.26	176.3	−113.7	70.9	0.5	5.5	3.1

Line

			Order		
	e		0	1	2
m_subsc_i	1.82	t_x	147.5	2.5	
		t_y	4.7	25.9	
		t_z	44.8	3.6	
m_supr_i	1.51	t_x	185.7	−26.1	
		t_y	47.8	1.6	
		t_z	76.2	−15.4	
m_infr_i	2.42	t_x	202.2	−13.5	
		t_y	23.0	27.2	
		t_z	70.3	−0.3	
m_ter_min_i	1.09	t_x	194.1	7.0	
		t_y	−8.6	33.4	
		t_z	52.8	8.8	
m_ter_maj_i	1.01	t_x	171.5	−7.9	
		t_y	−68.2	53.3	
		t_z	60.7	−3.9	
m_lat_dor_i	1.35	t_x	172.9	−12.1	
		t_y	−41.0	44.8	
		t_z	52.5	−7.2	
m_pec_maj_i	2.07	t_x	174.3	−2.4	
		t_y	−101.4	117.3	
		t_z	58.2	−22.0	
sulcus_bic	1.27	t_x	−11.3	−3.0	168.5
		t_y	−22.2	53.7	10.9
		t_z	40.5	−21.4	32.5

Sphere

	e	m_x	m_y	m_z	r
art_gh_hum	0.76	174.4	22.7	57.8	26.6
tub_minus + tub_majus	0.98	175.2	22.2	55.7	30.1

Cylinder

	e	x_0	y_0	d_x	d_y	d_z	r
Collum_hum	0.71	138.7	349.8	0.10	0.98	0.15	10.7

Point

	e	x	y	z
m_bic_i	0.65	195.5	−327.0	62.0
m_tric_i	0.97	207.3	−285.3	102.7
epic_med	—	180.1	−296.2	102.6
epic_lat	—	222.4	−291.8	59.5
olecranon	—	212.7	−297.2	102.1

articular surface to the other (maximal ±20 mm) and the effect of an articular disc (Fig. 3), the centroid of the plane fitted to the proximal joint surface can be assumed to be the rotation center of the joint. The orientation of the plane is important for decomposing joint reaction forces into a compressing component (perpendicular to the articular surface) and shearing components (parallel to the articular surface).

In the finite-element model, the scapulothoracic gliding plane is represented as a SURFACE element: a point of the scapula following the surface of the thorax. In this study, the scapulathoracic gliding plane has been modelled by an ellipsoid with its axes parallel to the main anatomical axes. The parameters of this ellipsoid are then the coordinates of the center of the ellipsoid and the lengths of its axes in x-, y- and

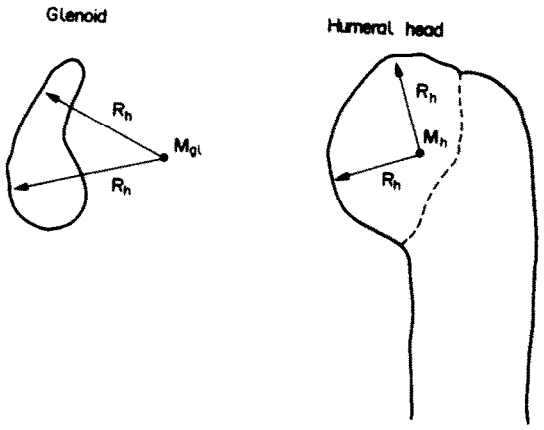

Fig. 2. The glenohumeral joint consists of the glenoid and the humeral head. The rotation center of the humerus with respect to the scapula is the center Mgl of the sphere fitted to the glenoid, using the radius Rh of the humeral head as radius. Mh: center of the sphere fitted to the humeral head; Rh: radius of the sphere fitted to the humeral head; Mgl: center of the sphere fitted to the glenoid with Rh as radius.

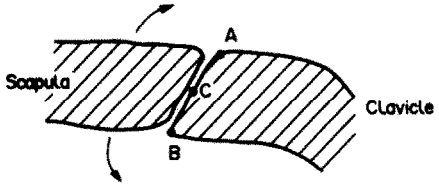

Fig. 3. The acromioclavicular joint between the clavicula and the scapula. If the small translations in the joint are neglected, then the rotation center of the scapula with respect to the clavicula, shifts from A to B, for upward and downward rotation, respectively. The error of the estimated rotation center C, the centroid of the clavicular joint surface, will be at most half the diameter of the joint surface.

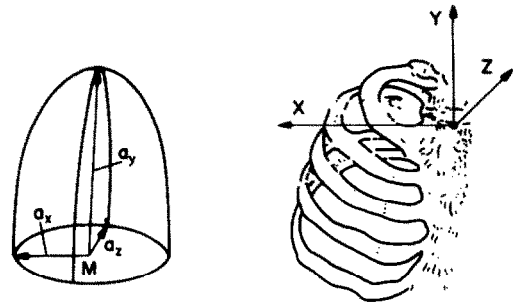

Fig. 4. The parameters of the ellipsoid fitted to the scapulothoracic gliding plane are the coordinates of the center of the ellipsoid (M_x, M_y, M_z) and the axes of the ellipsoid (a_x, a_y, a_z).

z-directions (Fig. 4). For stability of the iteration process and application in the finite-element method, the x-coordinate of the center of the ellipsoid is in the medial sagittal plane [$(x=0)$-plane].

A flat attachment site of a muscle or ligament is modelled as a plane. The parameters describing an attachment site are:

—the normal vector to the plane (n_x, n_y, n_z);

—the centroid of the attachment projected onto the plane (c_x, c_y, c_z);

—the distribution (first-order moment) of the attachment site in x-, y- and z-direction (d_x, d_y, d_z);

—the mean residual error $\bar{e}$ of the least-squares fit of the datapoints to the plane.

Example 1. Using normal vector $\mathbf{N}(n_x, n_y, n_z)$ and centroid $\mathbf{C}(c_x, c_y, c_z)$, an attachment plane can be described by

$$n_x c_x + n_y c_y + n_z c_z + D = 0,$$

from which D can be calculated. Distributions d_x, d_y and d_z show the sizes of the attachment site along the x-, y- and z-direction, respectively. The mean residual error is an indication of the correctness of the chosen model. Figure 5 shows the results of modelling the origin of m. subscapularis.

Other muscle attachments are modelled with a line parameterized as a function of variable t as $[x(t), y(t), z(t), 0 \leqslant t \leqslant 1]$. The parameters describing the polynome in t are, respectively, the vectors $\mathbf{t}_x$, $\mathbf{t}_y$ and $\mathbf{t}_z$. The order of the line equals the vector dimension minus one. When a muscle attachment is modelled as a point (e.g. in case of a tendon), simply the mean of the recorded datapoints can be presented.

Example 2. Using vectors $\mathbf{t}_x$, $\mathbf{t}_y$ and $\mathbf{t}_z$, an attachment line can be described as a function of $t(0 \leqslant t \leqslant 1)$:

$$x = \mathbf{t}_x(1) + \mathbf{t}_x(2) \cdot t + \mathbf{t}_x(3) \cdot t^2 + \cdots + \mathbf{t}_x(n) \cdot t^{n-1};$$

$$y = \mathbf{t}_y(1) + \mathbf{t}_y(2) \cdot t + \mathbf{t}_y(3) \cdot t^2 + \cdots + \mathbf{t}_y(n) \cdot t^{n-1};$$

$$z = \mathbf{t}_z(1) + \mathbf{t}_z(2) \cdot t + \mathbf{t}_z(3) \cdot t^2 + \cdots + \mathbf{t}_z(n) \cdot t^{n-1};$$

where $\mathbf{t}_x(1)$ is the first element of vector $\mathbf{t}_x$, etc. Start and end of the attachment line is given by $t=0$ and $t=1$, respectively. Figure 6 shows the results of modelling the origin of m. serratus anterior.

Beads were used to mark origin and insertion of some muscle bundles. For a numer of corresponding beads, x-, y- and z-coordinates of origin and insertion were recorded. After a line was fitted to the attachment, a t-value is assigned to each point at the attachment which was marked with a bead. Hence, for N beads, t-values at the origin $t_{oj} (j=1, \ldots, N)$ and t-values at the insertion t_{ij} are known. Next, t_{oj} is fitted to t_{ij}. This map can be used to interpolate the corresponding t-values of all fibers in between. Illustrations of such maps are presented in Fig. 7(a) and (b). Using maps like Fig. 7(a) and (b), in combination with Tables 2–5, the attachment site of any muscle bundle can be reconstructed.

Example 3. Starting with a t-value $t_{ok} (0 \leqslant t_{ok} \leqslant 1)$ at the origin of muscle bundle k, the corresponding value

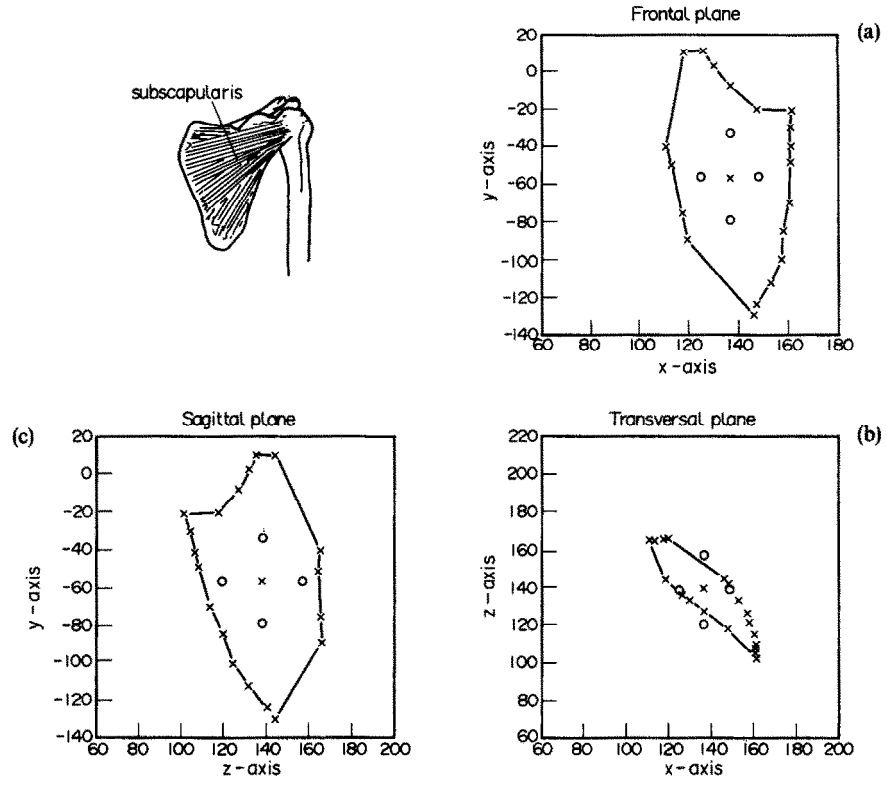

Fig. 5. Origin m. subscapularis at the scapula: (a) projection frontal plane; (b) projection transverse plane; (c) projection sagittal plane. (× . . . ×) recorded datapoints connected by a straight line; (×) centroid; (○) distribution with respect to the centroid.

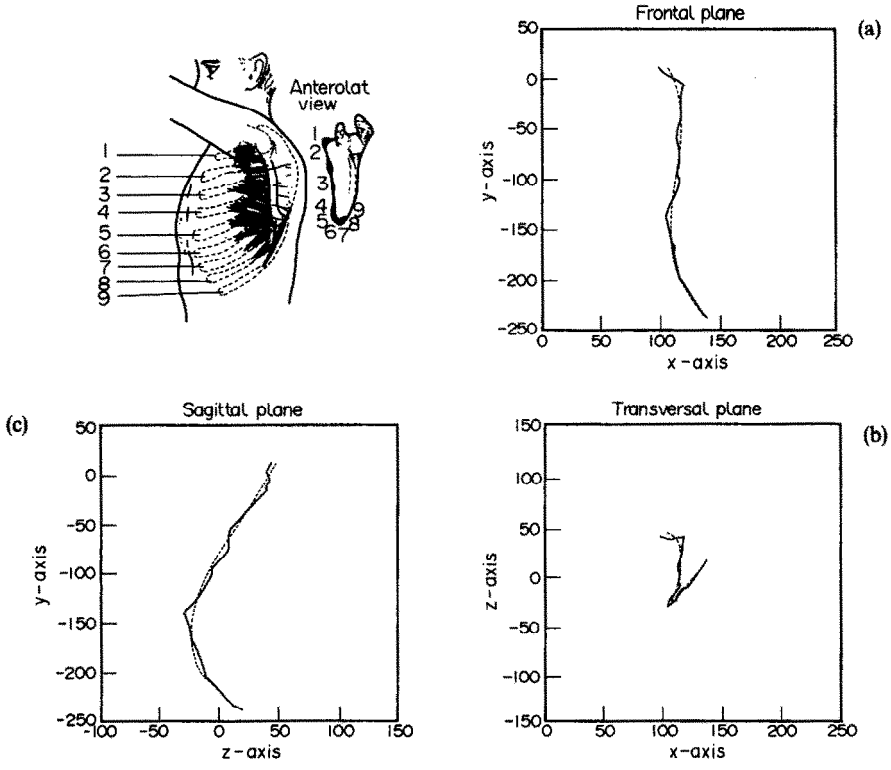

Fig. 6. Origin m. serratus anterior at the thorax (1 to 9: origin and insertion of distinct heads): (a) projection frontal plane; (b) projection transverse plane; (c) projection sagittal plane. (– – –) fitted to the datapoints; (———) connecting datapoints.

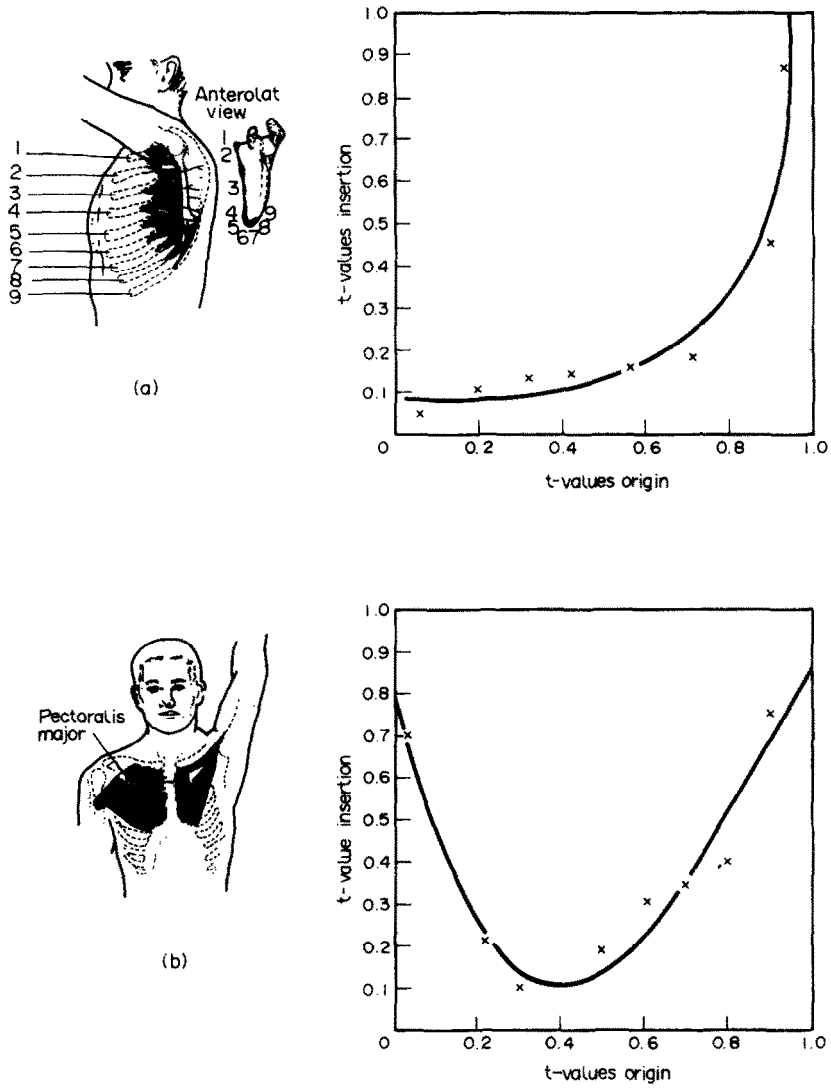

Fig. 7. Mapping of the t-values of the origin (t_0) to the t-values of the insertion (t_i), in order to obtain the direction of the muscle bundles: (a) m. serratus anterior; (b) m. pectoralis major.

t_{ik} at the insertion is found using the map from the origin to the insertion [Fig. 7(a) and (b)]. As explained in Example 2, t_{ok} and t_{ik} can be used to calculate the x-, y- and z-coordinates of origin and insertion of bundle k, respectively, using the appropriate vectors $\mathbf{t}_x$, $\mathbf{t}_y$ and $\mathbf{t}_z$, as presented in Tables 2–5. Path of the bundle is determined by a straight line between origin and insertion, or, in case a bony contour intervenes (Table 1), the shortest path around the bony contour is calculated.

Total force of a muscle is the summation of all forces of its bundles. Using the data of this study, a general theory is developed for representing the mechanical effect of the whole muscle with an adequate number of muscle lines of action. Figure 8(a) shows the position and directon of a large number of muscle bundles of m. trapezius, Fig. 8(b) shows the position and direction of six muscle lines of action which are necessary to represent the mechanical effect (Van der Helm and Veenbaas, 1991).

Some bony contours determine the muscle path (Table 1). The thorax is modelled as an ellipsoid, the tuberculum majus, combined with the tuberculum minus, as a sphere, the caput humeri also as a sphere and the humeral shaft as a cylinder. The parameters of the cylinder are the direction vector of the axis (d_x, d_y, d_z), the position of the axis $[x_0, y_0, (z_0=0)]$ and the radius r (Fig. 9).

The muscle path is defined as the shortest line between origin and insertion, which will be a straight line if no bony contour intervenes. Otherwise, the shortest path around the bony contour can be calculated from the position coordinates of origin and insertion and the mathematical description of the surface of the bony contour. In the finite-element method, each muscle line of action is represented by

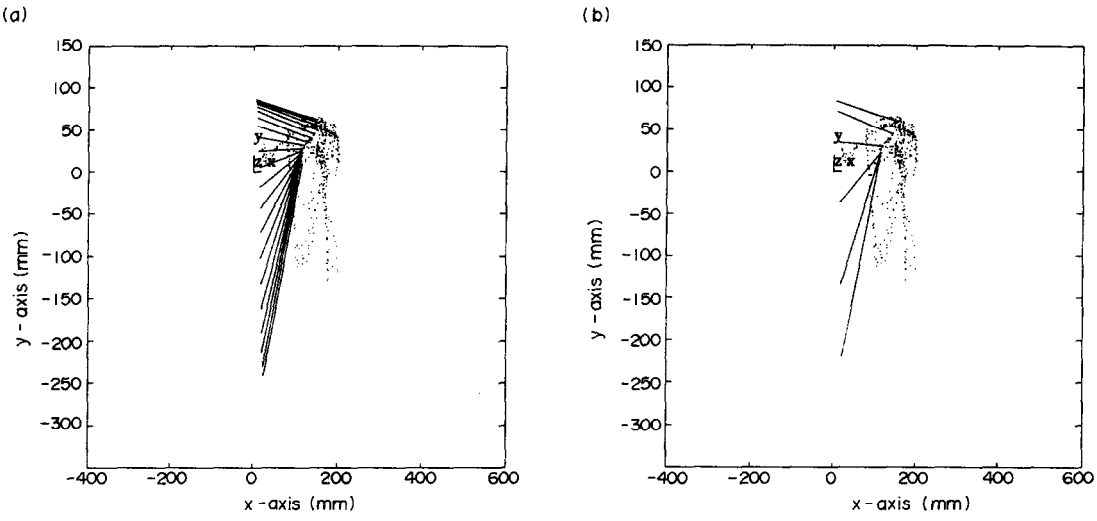

Fig. 8. Representation of the mechanical effect of the scapular part of m. trapezius by multiple muscle lines of action: (a) 20 muscle lines of action; (b) 6 muscle lines of action (as used in the finite-element model).

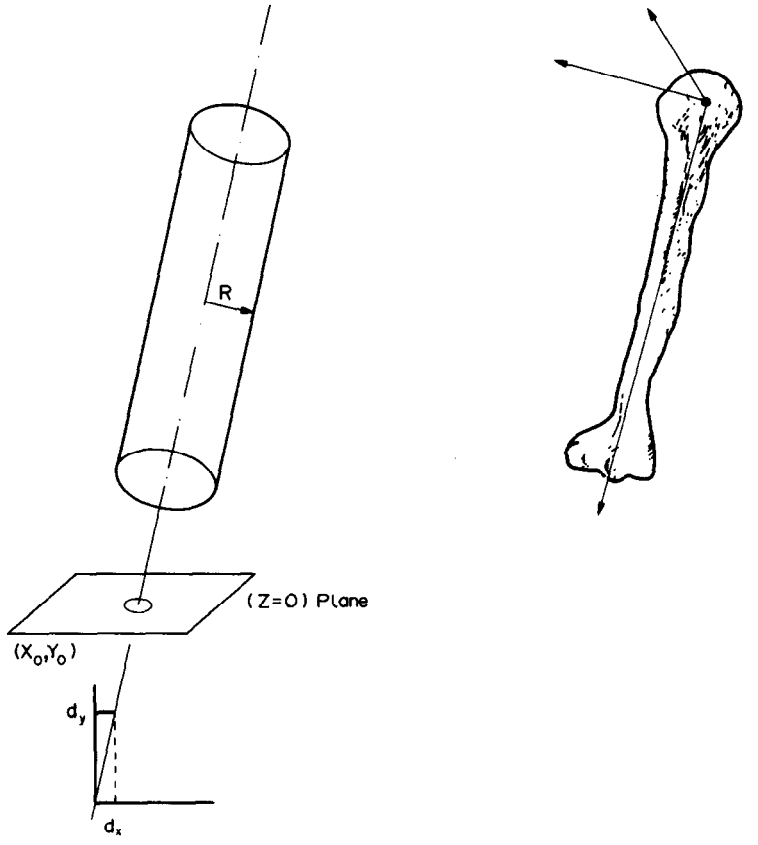

Fig. 9. The parameters of the cylinder fitted to the collum humeri are the normalized direction vector (d_x, d_y) of the central line through the cylinder, the intersection of the central line and the $(z=0)$-plane (x_0, y_0) and the radius r of the cylinder.

an active element. Origin and insertion are rigidly connected to any local coordinate system of the bone. Motion of the local coordinate system is determined by motion of bony landmarks, which are also rigidly attached. Hence, starting from the position in which the cadaver was measured, new positions can easily be calculated using rigid-body kinematics. In each new position, muscle lines of action are recalculated,

whether or not wrapped around bony contours, which, in turn, are rigidly attached to the local coordinate systems.

No explicit data about muscle length and moment arms are presented in this article, since these data will change with each position of the shoulder mechanism. It is more important to consider that muscle length and moment arms can be derived for any position, using a model of the shoulder mechanism.

DISCUSSION

In order to obtain 3-D coordinates, the palpator is used (Pronk and Van der Helm, 1991). This instrument permitted a new experimental method. Firstly, positions of bony segments (thorax, clavicula, scapula and humerus) were measured in a global coordinate system by means of six screws fastened to the bones. After dissection and exarticulation, a large number of datapoints at each morphological structure were measured in a local coordinate system. The configuration of screws has been used to calculate a transformation function from the local to the global coordinate system. This transformation introduces an additional error (residual error $\bar{e}$ of the estimation of the transformation function) in repositioning the bony segments with respect to each other, about 1–3 mm for each segment (Veeger *et al.*, 1991).

Using the palpator, a large number of datapoints could be recorded. From the datapoints collected mathematical descriptions of each morphological structure can be derived. Three-dimensional geometrical forms are used for mathematical description. The choice of a certain form is rather subjective, mainly directed by an optical resemblance. The residual error of the fitting procedure, which is small for all structures, is the only justification afterwards (see Tables 2–5).

The experimental method of this study enabled a recording of all important morphological structures: muscle attachments, joint surfaces, bony contours, bundle orientations, ligament attachments and bony landmarks. From the position and shape of the articular surface, the position of joint rotation centers as well as the direction of compression and shear joint reaction forces can be calculated. In our finite-element model, the medial border of the scapula is constrained to follow the scapulothoracic gliding plane. For each muscle, the position of the whole attachment site of origin and insertion is modelled. Combined with the bundle orientation and, eventually, the bony contour underneath a muscle, a number of (curved) muscle lines of action are calculated, which adequately represent the muscle action for each position of the muscle. In this way, the muscle moment arm can be calculated. The same approach as for muscles is applicable for ligaments, except that dimensions of ligaments are so small that one line of action is considered to be sufficient. Combined with mass and moment of inertia of segments, an inverse dynamical analysis can be performed, using PCSA as an estimate of the maximal muscle force and a suitable optimization criterion to calculate muscle force. In addition, a number of bony landmarks are recorded. Motions of the shoulder mechanism were recorded using these bony landmarks (Pronk, 1987). The advantage of such an approach in musculoskeletal modelling is clear: for each new position of the bony segments, the position of the rotation center of the joints, the muscle attachments and the bony contours can be calculated again. Hence, the new muscle lines of action and moment arms can be assessed for each position of the shoulder mechanism. A disadvantage of this method is that, for curved muscle lines of action, the diameter of muscles is neglected. However, the muscles in the shoulder mechanism concerned are flat muscles, so the systematic error is likely to be small.

The shoulder mechanism of each individual performs more or less the same functions. It could be that the same morphology is a basis for these functions. It is, however, possible that the same functions can be performed with different mechanisms. This would imply that the shoulder mechanism can only be compared on a functional level, and not on the underlying morphology. The geometry parameters derived in this study for both shoulders of seven cadavers, were not sufficiently similar to allow them to be presented as averages over all cadavers.

Therefore, we are inclined to state that the geometry of each muscle should be regarded in comparison with the geometry of the whole shoulder, which means that only functional aspects of morphology can be compared.

CONCLUDING REMARKS

(1) In this study, a complete parameter set, consisting of inertia, geometry and muscle parameters, of the shoulder mechanism is derived for seven cadavers. It will be possible to make comparisons between individuals on a morphological and functional level.

(2) The data are mathematically described by geometrical forms, which can be incorporated in a dynamical finite-element model of the shoulder mechanism.

(3) Through the assessment of muscle architecture, i.e. bundle direction, and the description of the whole attachment area, an adequate number of force vectors can be positioned in order to represent muscle action.

(4) Since the location of muscle attachments, rotation centers and bony contours can be recalculated after motion of the bones, moment arms and mechanical effects of muscles can be determined for any position of the shoulder mechanism.

REFERENCES

Bassett, R. W., Browne, A. O., Morrey, B. F. and An, K. N. (1990) Glenohumeral muscle force and moment mechanics

in a position of shoulder instability. *J. Biomechanics* **23,** 405–415.
Brand, R. A., Crowninshield, R. D., Wittstock, C. E., Pederson, D. R., Clark, C. R. and van Krieken, F. M. (1982) A model of lower extremity muscular anatomy. *ASME J. biomech. Engng* **104,** 304–310.
De Luca, C. J. and Forrest, W. J. (1973) Force analysis of individual muscles acting simultaneously on the shoulder during isometric abduction. *J. Biomechanics* **6,** 385–393.
Entken, P. J. M. and Wijgergangs, G. K. (1984) Three-dimensional definition of both the shape of the thoracic wall and the positions of the scapula and clavicle at humerus abduction (in Dutch). Rep. N-228, Lab. WBMR, Delft Univ. Techn., Delft, The Netherlands.
Fick, R. (1911) *Handbuch der Anatomie und Mechanik der Gelenke*, Teil 3. Gustav Fischer, Jena.
Gracovetsky, S. and Farfan, H. (1986) The optimum spine. *Spine* **11,** 543–573.
Gracovetsky, S., Farfan, H. and Lamy, C. (1981) The mechanism of the lumbar spine. *Spine* **6,** 249–262.
Hogfors, C., Sigholm, G. and Herberts, P. (1987) Biomechanical model of the human shoulder—I. Elements. *J. Biomechanics* **20,** 157–166.
Hvorslev, C. M. (1927) Studien ueber die Bewegungen der Schulter. *Skand. Arch. f. Physiol.* (separatabdruck).
Inman, V. T., Saunders, J. B. and Abbot, L. C. (1944) Observations on the function of the shoulder joint. *J. Bone Jt Surg.* **26-A,** 1–30.
Jonker, B. (1988) A finite element dynamical analysis of flexible spatial mechanisms and manipulators. Doctoral thesis, Delft Univ. Techn., Delft, The Netherlands.
Levenberg, K. (1944) A method for the solution of certain nonlinear problems in least squares. *Quart. Appl. Math.* **2,** 164–168.
Ljung, L. (1987) *System Identification: Theory for the User.* Prentice-Hall, New Jersey.
Marquardt, D. W. (1963) An algorithm for least squares estimation of nonlinear parameters. *SIAM J. appl. Math.* **11,** 431–441.
Mollier, S. (1899) Ueber die Statik und Mechanik des menslichen Schultergurtels unter normalen und pathologischen Verhaltnissen. Festschr. f.c. v. Kupfer, Jena.
Pierrynowski, M. R. (1982) A physiological model for the solution of individual muscle forces during normal human walking. Ph.D. thesis, Simon Fraser University.
Poppen, N. K. and Walker, P. S. (1978) Forces at the glenohumeral joint in abduction. *Clin. Orthop. Rel. Res.* **135,** 165–170.
Pronk, G. M. (1987) Three-dimensional determination of the position of the shoulder girdle during humerus elevation. Biomechanics XI-B: 1070-1076, 11th ISB-Congress, Amsterdam.
Pronk, G. M. (1989) A kinematic model of the shoulder girdle: a resume. *J. Med. Engng Technol.* **13,** 119–123.
Pronk, G. M. and Padt, A. Van der (1986) The modelling of the scapulothoracic wall. Rep. N-245, Lab. WBMR, Delft Univ. Techn., Delft, The Netherlands.
Pronk, G. M. and Van der Helm, F. C. T. (1991) The palpator, an instrument for measuring the three-dimensional positions of bony landmarks in a fast and easy way. *J. Med. Engng Technol.* **15**(1), 15–20.
Scholten, P. J. M., de Boer, A. and Vuisting, W. (1982) A biomechanical analysis of the functions of the deltoid during abduction of the arm. *Engng Med.* **11,** 3–10.
Schultz, P. (1985) Model validation of the scapulothoracic gliding plane (in Dutch). Rep. S-374, Lab. WBMR, Delft Univ. Techn., Delft, The Netherlands.
Seireg, A. and Arvikar, R. J. (1975) The prediction of muscular load sharing and joint forces in the lower extremities during walking. *J. Biomechanics* **8,** 89–102.
Shiino, K. (1913) Schultergelenkbewegungen und Schultermuskelarbeit. *Arch. Anat. Physiol., Suppl. Anat. Abtlg.*, 1–88.
Van der Helm, F. C. T. (1988) A dynamic model of the shoulder girdle. In *Abstracts: 6th Meeting of the European Society of Biomechanics*, abstract No. B26, Bristol, England.
Van der Helm, F. C. T. and Pronk, G. M. (1989) A finite element musculoskeletal model of the shoulder mechanism. Presented at 2nd Int. Symp. com. Simul. in Biomech., Davis, CA, 1989.
Van der Helm, F. C. T., Pronk, G. M., Veeger, H. E. J. and Van Der Woude, L. H. V. (1989) The rotation center of the glenohumeral joint. In *Proc. 12th ISB-Congr.* (Edited by Gregor, R. J., Zernicke, R. F. and Whiting, W. C.), UCLA, pp. 676–677. Los Angeles, U.S.A.
Van der Helm, F. C. T. and Veenbaas, R. (1991) Modelling the mechanical effect of muscle with large attachment sites: application to the shoulder mechanism. *J. Biomechanics* **24**(12), 1151–1163.
Van Huffel, S. and Vandewalle, J. (1985) The use of total linear least squares techniques for identification and parameter estimation. In *Proc. IFAC, Ident. Syst. Par. Est.*, Vol. 2-C, pp. 1167–1172.
Veeger, H. E. J., Van der Helm, F. C. T., Van Der Woude, L. H. V. and Pronk, G. M. (1991) Inertia and muscle contraction parameters for musculoskeletal modelling of the shoulder mechanism. *J. Biomechanics* **24**(7), 615–629.
Werff, K. van der (1977) Kinematic and dynamic analysis of mechanisms: A finite element approach. Doctoral thesis, Delft University of Technology, The Netherlands.
Werff, K. van der and Jonker, B. (1983) Dynamics of flexible mechanisms. In *Proc. NATO Advanced Study Inst. on Computer Aided Analysis and Optimization of Mechanical System Dynamics*, Iowa City, pp. 381–400.
Woittiez, R. D. (1984) A quantitative study of muscle architecture and muscle function. Ph.D. thesis, Free Univ. Amsterdam, The Netherlands.
Wood, J. E., Meek, S. G. and Jacobsen, S. C. (1989a) Quantification of human shoulder anatomy for prosthetic arm control I. Surface modelling. *J. Biomechanics* **22,** 273–292.
Wood, J. E., Meek, S. G. and Jacobsen, S. C. (1989b) Quantification of human shoulder anatomy for prosthetic arm control II. Anatomy matrices. *J. Biomechanics* **22,** 319–325.

APPENDIX A
PARAMETER ESTIMATION OF A PLANE

The general mathematical description of a plane in 3-D space is

$$Ax + By + Cz + 1 = 0. \tag{A1}$$

Fitting a plane to a number of measured datapoints is defined as minimizing the distance of the datapoints to the plane with a quadratic criterion. By virtue of the fact that the equation of a plane is linear, the total linear least-squares (TLLS) technique for parameter estimation can very elegantly be used (Van Huffel and Vandewalle, 1985). One important feature of this technique is that the noise will be distributed over all position coordinates of the datapoints, in contradiction to an ordinary linear least-squares solution, which will attribute all the measurement noise to one coordinate.

The equation mentioned above can be rewritten in matrix form as

$$\begin{bmatrix} x_1 & y_1 & z_1 & 1 \\ \vdots & \vdots & \vdots & \vdots \\ x_N & y_N & z_N & 1 \end{bmatrix} \begin{bmatrix} A \\ B \\ C \\ 1 \end{bmatrix} = \mathbf{0} \text{ or } Z_N\theta = \mathbf{0}, \tag{A2}$$

where (x_i, y_i, z_i) are the position coordinates of datapoint i, Z_N is the matrix of N datapoints, and θ the parameter vector $(A, B, C, 10^{-6})$.

In general, this equation will not have a solution for the parameter vector θ. Therefore, Z_N will be slightly deviated to $\hat{Z}_N$ to get a solution for θ

$$\hat{Z}_N \cdot \theta = 0 \quad \text{or} \quad \begin{bmatrix} \hat{x}_1 & \hat{y}_1 & \hat{z}_1 & 1\hat{0}^6 \\ \vdots & \vdots & \vdots & \vdots \\ \hat{x}_N & \hat{y}_N & \hat{z}_N & 1\hat{0}^6 \end{bmatrix} \begin{bmatrix} A \\ B \\ C \\ 10^{-6} \end{bmatrix}. \quad \text{(A3)}$$

The TLLS technique will minimize the Frobenius norm

$$\| Z_N - \hat{Z}_N \|_F = \sqrt{\sum_{ij} (Z_{N_{ij}} - \hat{Z}_{N_{ij}})^2}. \quad \text{(A4)}$$

The last column of Z_N is scaled to 10^6 to minimize the attribution of noise to this column. The parameter vector θ is obtained by the TLLS technique as follows.

The singular-value decomposition (SVD) is denoted by

$$\text{SVD}(Z_N) = U \cdot \Sigma \cdot V^T, \quad \text{(A5)}$$

where U represents left-singular vectors and V the right-singular vectors;

$$\Sigma = \begin{bmatrix} \text{diag}(\sigma_1 \cdots \sigma_4) \\ 0 \end{bmatrix},$$

where $\text{diag}(\sigma \ldots \sigma_4)$ is the diagonal matrix with the singular values, $\sigma_1 \geqslant \sigma_2 \geqslant \sigma_3 \geqslant \sigma_4$.

To get a minimal deviation $[\hat{Z}_N]$, σ_4 is replaced by zero. Then,

$$\hat{Z}_N = U \cdot \hat{\Sigma} \cdot V^T \quad \text{(A6)}$$

$$\hat{Z}_N \cdot \theta = 0, \quad \text{(A7)}$$

where

$$\hat{\Sigma} = \begin{bmatrix} \text{diag}(\sigma_1 \cdots \sigma_3 0) \\ 0 \end{bmatrix}.$$

The TLLS solution for θ is obtained by scaling the last row $\mathbf{R}_4$ of V^T until its last component is 10^{-6}:

$$\theta = \left(\frac{\mathbf{R}_4}{V(4,4)} \right) 10^{-6}. \quad \text{(A8)}$$

APPENDIX B
PARAMETER ESTIMATION OF A SPHERE

In order to model the glenohumeral joint surfaces as a perfect sphere, the measured positions of about 50 points on these surfaces were fitted to a mathematical description of a sphere, by minimizing the distance e_i of each point (x_i, y_i, z_i) to the sphere with radius r and center (m_x, m_y, m_z),

$$e_i = \sqrt{(x_i - m_x)^2 + (y_i - m_y)^2 + (z_i - m_z)^2} - r. \quad \text{(B1)}$$

Using a quadratic criterion, this yields, for N datapoints, the minimization of

$$V_N(\theta, Z_N) = \frac{1}{N} \sum_{i=1}^{N} \frac{1}{2} e_i^2(\theta), \quad \text{(B2)}$$

where θ is the parameter vector containing m_x, m_y, m_z, r, and Z^N the set of datapoints (x_i, y_i, z_i), $i = 1, \ldots, N$.

This is a nonlinear least-squares problem, which can be solved by an iterative Gauss–Newton method (Ljung, 1987).

To obtain a first estimate, $\hat{\theta}_N^{(0)}$ of the parameter vector, the following description of a sphere is used:

$$A(x^2 + y^2 + z^2) + Bx + Cy + Dz + E = 0, \quad \text{(B3)}$$

which is linear in the parameters. The parameters of this equation can be solved by using the total linear least-squares method (Van Huffel and Vandewalle, 1985); see Appendix A.

APPENDIX C
PARAMETER ESTIMATION OF AN ELLIPSOID

Earlier studies have showed that the thorax, and, in particular, the scapulothoracic gliding plane, can be modelled by an ellipsoid (Entken and Wijgergangs, 1984; Schultz, 1985; Pronk and Padt, 1986). In this study, the scapulothoracic gliding plane as well as the muscle path of the m. serratus anterior are approximated by an ellipsoid. To find a best fit with the ellipsoid, the distance between the measured datapoints and the ellipsoid is minimized using a quadratic criterion. For the sake of convenience in calculation, the axes of the ellipsoid are placed in the coordinate planes. To obtain a stable algorithm, the x-coordinate of the center of the ellipsoid is chosen to be in the $(x = 0)$-plane.

The equation of such an ellipsoid is

$$\left[\frac{x - m_x}{a_x} \right]^2 + \left[\frac{y - m_y}{a_y} \right]^2 + \left[\frac{z - m_z}{a_z} \right]^2 = 1, \quad \text{(C1)}$$

where x, y, z are coordinates of points on the ellipsoid, m_x, m_y, m_z are coordinates of the center of the ellipsoid $(m_x = 0)$, and a_x, a_y, a_z are axes of the ellipsoid in the x-, y- and z-direction, respectively.

The shortest distance between a point i (x_i, y_i, z_i) and the ellipsoid is along a normal of the ellipsoid through i, intersecting the ellipsoid at i' (x_i', y_i', z_i'). Then the line through the points i and i' is described by the equation

$$\begin{bmatrix} x_i \\ y_i \\ z_i \end{bmatrix} = \begin{bmatrix} x_i' \\ y_i' \\ z_i' \end{bmatrix} + \mu_i \begin{bmatrix} \frac{2(x_i' - m_x)}{a_x^2} \\ \frac{2(y_i' - m_y)}{a_y^2} \\ \frac{2(z_i' - m_z)}{a_z^2} \end{bmatrix}. \quad \text{(C2)}$$

Combining equations (C2) and (C1) results in function $F(\mu_i)$,

$$F(\mu_i) = \left[\frac{x_i - m_x}{a_x + 2\mu_i / a_x} \right]^2 + \left[\frac{y_i - m_y}{a_y + 2\mu_i / a_y} \right]^2 + \left[\frac{z_i - m_z}{a_z + 2\mu_i / a_z} \right]^2 - 1. \quad \text{(C3)}$$

For a given set of ellipsoid parameters and a datapoint $i(x_i, y_i, z_i)$, μ_i can be solved from this equation when $F(\mu_i)$ is zero, and, with equation (C2), the coordinates of point i' can be calculated. Consequently, the distance between i and i' is the distance from i to the ellipsoid.

An initial approximation of μ_i is achieved by a stepping routine. μ_i is solved numerically by an iterative Taylor expansion:

$$\mu_i^{(j+1)} = \mu_i^{(j)} + \left[\frac{\delta F(\mu_i)}{\delta \mu_i} \right]^{-1} \Delta F(\mu_i) + \frac{1}{2} \left[\frac{\delta^2 F(\mu_i)}{\delta \mu_i^2} \right]^{-1} \Delta F(\mu_i)^2, \quad \text{(C4)}$$

where $\Delta F(\mu_i) = [F_0(\mu_i) - F(\mu_i)]$, $F_0(\mu_i) = 0$, and $\mu_i^{(j)}$ is the jth update of μ_i.

An estimation of the center and the axes of the ellipsoid is obtained by minimizing the criterion

$$V_N(\theta, Z_N) = \frac{1}{N} \sum_{i=1}^{N} \frac{1}{2} e_i^2(\theta), \quad \text{(C5)}$$

θ is parameter vector containing m_y, m_z, a_x, a_y, a_z, and Z_N is the set of datapoints.

The next procedure is a modification of the Gauss–Newton method as described in Appendix B. The approximation of the Hessian $V''(\hat{\theta}_N^{(j)}, Z_N)$ happens to be close to singular because the data are not informative

enough (only data of one side of the ellipsoid are obtained!). One way to overcome this problem is the application of the Levenberg–Marquardt procedure (Levenberg, 1944; Marquardt, 1963). In addition, a turbo-parameter f is used to enforce a line search as long as the criterion $V_N(\theta, Z_N)$ decreases. For each successful step, f is increased by a factor of 2. This reduces the number of calculations of the gradient and thus improves the speed of the algorithm:

$$\hat{\theta}_N^{(j+1)} = \hat{\theta}_N^{(j)} - f[V''(\hat{\theta}_N^{(j)}, Z_N] + \alpha \operatorname{diag}\{V''(\hat{\theta}_N^{(j)}, Z_N)\}]^{-1} V'(\hat{\theta}_N^{(j)}, Z_N), \quad \text{(C6)}$$

where α is Marquardt parameter (initially equal to 0.01; increased by a factor of 4 if a step is not successful; decreased by a factor 8 if a step is successful), $V'(\hat{\theta}_N^{(j)}, Z_N)$, is the gradient of the criterion with respect to parameter vector $\hat{\theta}_N^{(j)}$ at the jth iterate, and $V''(\hat{\theta}_N^{(j)}, Z_N)$ is the Hessian of the criterion.

To obtain a first estimate $\theta_N^{(0)}$ of the parameter vector, the following description of an ellipsoid is used:

$$Ax^2 + By^2 + Cz^2 + Dx + Ey + Fz + 1 = 0, \quad \text{(C7)}$$

which is linear in the parameters. This equation can be solved for the parameters, using the total linear least-squares (TLLS) technique (Van Huffel and Vandewalle, 1985); see Appendix A.

$$\begin{bmatrix} x_1^2 & y_1^2 & z_1^2 & x_1 & y_1 & z_1 & 10^6 \\ \vdots & \vdots & \vdots & \vdots & \vdots & \vdots & \vdots \\ x_N^2 & y_N^2 & z_N^2 & x_N & y_N & z_N & 10^6 \end{bmatrix} \begin{bmatrix} A \\ B \\ C \\ D \\ E \\ F \\ 10^{-6} \end{bmatrix} = \mathbf{0}. \quad \text{(C8)}$$

Equation (C1) can be rewritten in the form of equation (C7):

$$\frac{1}{a_x^2}x^2 + \frac{1}{a_y^2}y^2 + \frac{1}{a_z^2}z^2 - \frac{2m_x}{a_x^2}x - \frac{2m_y}{a_y^2}y - \frac{2m_z}{a_z^2}z + \frac{m_x^2}{a_x^2} + \frac{m_y^2}{a_y^2} + \frac{m_z^2}{a_z^2} - 1 = 0. \quad \text{(C9)}$$

APPENDIX D
PARAMETER ESTIMATION OF A CYLINDER

One common feature of all points on the surface of a cylinder is that they have equal distance to the central axis of the cylinder. If we characterize this central axis by

$$\begin{bmatrix} x \\ y \\ z \end{bmatrix} = \begin{bmatrix} x_0 \\ y_0 \\ z_0 \end{bmatrix} + \lambda \cdot \begin{bmatrix} d_x \\ d_y \\ d_z \end{bmatrix}, \quad \text{(D1)}$$

then the distance between a point i (x_i, y_i, z_i) and this line is given by

$$d_i^2 = \{[(x_i - x_0)d_y - (y_i - y_0)d_x]^2 + [(y_i - y_0)d_z - (z_i - z_0)d_y]^2 + [(z_i - z_0)d_x - (x_i - x_0)d_z]^2\} \times \left\{\frac{1}{d_x^2 + d_y^2 + d_z^2}\right\}. \quad \text{(D2)}$$

The direction vector (d_x, d_y, d_z) is a unit vector; thus,

$$d_z = \sqrt{1 - d_x^2 - d_y^2}. \quad \text{(D3)}$$

For the position vector (x_0, y_0, z_0), the intersection of the central axis and the $(z=0)$-plane is chosen; thus, $z_0 = 0$.

The distance of point i to the surface of the cylinder is expressed as

$$e_i = d_i - r = \sqrt{[(x_i - x_0)d_y - (y_i - y_0)d_x]^2 + [(y_i - y_0)\sqrt{1 - d_x^2 - d_y^2} - z_i d_y]^2 + [z_i d_x - (x_i - x_0)\sqrt{1 - d_x^2 - d_y^2}]^2} - r. \quad \text{(D4)}$$

An estimation of the central axis and the radius of the cylinder is obtained by minimizing the criterion

$$V_N(\theta, Z_N) = \frac{1}{N}\sum_{i=1}^{N} \frac{1}{2} e_i^2(\theta), \quad \text{(D5)}$$

θ is parameter vector containing d_x, d_y, x_0, y_0, R and Z_N is the set of datapoints.

This nonlinear least-squares proboem can be solved by an iterative Gauss–Newton method (see Appendix B) using turbo-parameter f (see Appendix C).

To obtain a first estimate $\theta_N^{(0)}$ of the parameter vector, a straight line is fitted to the datapoints (see Appendix E). This line is the first estimate of the central axis; the mean distance to the line is an estimate of the radius.

APPENDIX E
PARAMETER ESTIMATION OF A 3-D POLYNOMIAL

The x-, y- and z-coordinates of a (curved) line are expressed as a polynomial in variable t, with $t \in [0, 1]$:

$$\begin{aligned} x &= a_0 + a_1 t + a_2 t^2 + \cdots + a_n t^n, \\ y &= b_0 + b_1 t + b_2 t^2 + \cdots + b_n t^n, \\ z &= c_0 + c_1 t + c_2 t^2 + \cdots + c_n t^n, \end{aligned} \quad \text{(E1)}$$

or, in matrix form,

$$X = T\theta;$$

$$\begin{bmatrix} x_1 & y_1 & z_1 \\ x_2 & y_2 & z_2 \\ \vdots & \vdots & \vdots \\ x_N & y_N & z_N \end{bmatrix} = \begin{bmatrix} 1 & t_1 & t_1^2 & \cdots & t_1^n \\ 1 & t_2 & t_2^2 & \cdots & t_2^n \\ \vdots & \vdots & \vdots & & \vdots \\ 1 & t_N & t_N^2 & \cdots & t_N^2 \end{bmatrix} \begin{bmatrix} a_0 & b_0 & c_0 \\ a_1 & b_1 & c_1 \\ \vdots & \vdots & \vdots \\ a_n & b_n & c_n \end{bmatrix}, \quad \text{(E2)}$$

where x_i, y_i, z_i, are coordinates of datapoints $i (i = 1, \ldots, N)$, N is number of datapoints, t_i is the t-values of datapoint i, $0 < t_i \leq 1$, and a_j, b_j, c_j are parameters of a 3-D polynomial in t of order n $(j = 0, \ldots, n)$.

First, the datapoints i are sorted in the sequence of the attachment. The difference between t_i and t_{i+1} is proportional to the distance between the measured datapoints $\mathbf{p}_i$ and $\mathbf{p}_{i+1}$ with respect to the total length of the attachment site. The parameter matrix θ can easily be obtained by minimizing the least-squares criterion:

$$\theta = (T^T T)^{-1} T^T X. \quad \text{(E3)}$$